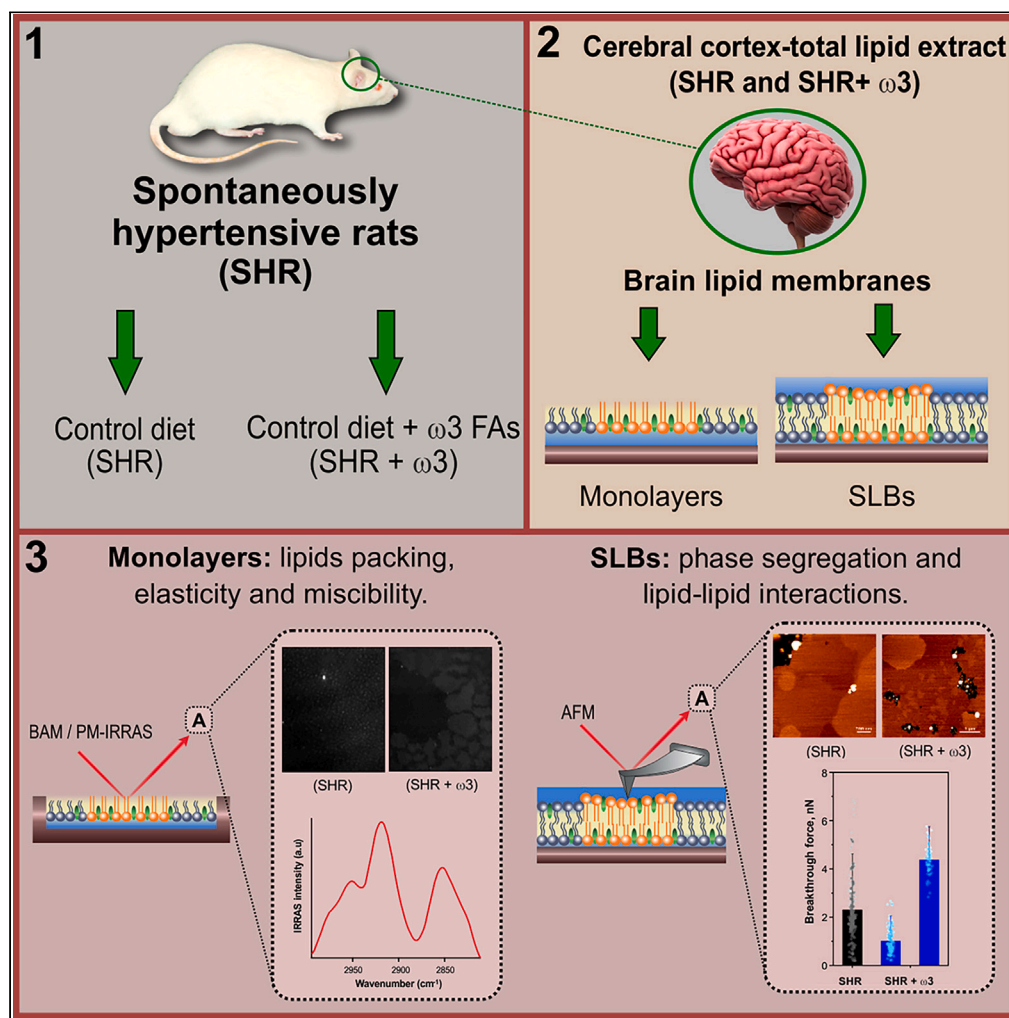**Article**

Understanding the effects of omega-3 fatty acid supplementation on the physical properties of brain lipid membranes

María L. Longarzo, Romina F. Vázquez, María J. Bellini, ..., Osvaldo N. Oliveira Jr, María L. Fanani, Sabina M. Maté

smate@med.unlp.edu.ar

Highlights

ω3 FAs alters brain lipid membranes, at molecular and nanoscale levels

ω3 FAs induce changes in molecular packing, elasticity, and lipid miscibility

ω3 FAs increase lipid phase disparity

Future research aims to unveil how ω3 levels influence cognition and behavior

Article

Understanding the effects of omega-3 fatty acid supplementation on the physical properties of brain lipid membranes

María L. Longarzo,[1,10] Romina F. Vázquez,[1,10] María J. Bellini,[1] Ricardo A. Zamora,[2,3] Lorena Redondo-Morata,[4] Marina I. Giannotti,[2,5,6] Osvaldo N. Oliveira Jr,[7] María L. Fanani,[8,9] and Sabina M. Maté[1,11,*]

SUMMARY

A deficiency in omega-3 fatty acids (ω3 FAs) in the brain has been correlated with cognitive impairment, learning deficiencies, and behavioral changes. In this study, we provided ω3 FAs as a supplement to spontaneously hypertensive rats (SHR+ ω3). Our focus was on examining the impact of dietary supplementation on the physicochemical properties of the brain-cell membranes. Significant increases in ω3 levels in the cerebral cortex of SHR+ ω3 were observed, leading to alterations in brain lipid membranes molecular packing, elasticity, and lipid miscibility, resulting in an augmented phase disparity. Results from synthetic lipid mixtures confirmed the disordering effect introduced by ω3 lipids, showing its consequences on the hydration levels of the monolayers and the organization of the membrane domains. These findings suggest that dietary ω3 FAs influence the organization of brain membranes, providing insight into a potential mechanism for the broad effects of dietary fat on brain health and disease.

INTRODUCTION

ω3 FAs are polyunsaturated acids with a double bond (C=C) at the third carbon atom from the terminal methyl group of the hydrocarbon chain. They cannot be synthesized *de novo* in humans, so they must be ingested with the diet or synthesized from dietary α-linolenic acid.[1] ω3 FAs have been studied for their effects on various aspects of health, including brain function. There is evidence that dietary and supplemental ω3 FAs have a protective effect against cognitive impairment. Docosahexaenoic acid (DHA) is an ω3 FA that accounts for ∼20% of the total membrane FAs in the central nervous system and is essential for the formation of neuronal networks and regulation of cell survival.[2,3] A decrease in DHA content is associated with cognitive impairment, learning deficits, and other behavioral alterations.[4] The effects of ω3 FAs on the brain are complex and multifaceted, most of which are still not fully understood. Synaptic plasticity, neuroinflammation, and changes in expression of genes linked to cognitive decline have been identified as potential targets of ω3 FAs.[1,4] DHA has been observed to accumulate in neuronal membranes, contributing to neuronal survival and functional maintenance through translocation and activation of Raf[5] and Akt,[6] which inhibits neuronal apoptosis.[7] DHA-derived resolvin (Rv) D1, neuroprotectin D1 (NPD1), and maresin-1, also known as specialized pro-resolving lipid mediators, have neuroprotective and anti-inflammatory effects and can block cognitive impairment and prevent dementia.[8,9]

The physicochemical properties of brain cell membranes are believed to be influenced by ω3 FAs in several ways. These FAs may affect the localization and activity of key proteins or key protein-lipid interactions in specific membrane domains and thereby affect signaling cascades, cell functions and, ultimately, brain health.[10] Studies into synthetic lipid mixtures showed that DHA influence acyl chain order and fluidity, phase behavior, elastic compressibility, permeability, fusion, and flip-flop.[11–16] Synthetic lipid mixtures can provide valuable insights into the fundamental properties of membranes and help researchers understand membrane-related phenomena. However, they are not exact

[1]Instituto de Investigaciones Bioquímicas de La Plata (INIBIOLP), CCT- La Plata, CONICET, Facultad de Ciencias Médicas, Universidad Nacional de La Plata, 60 y 120, (1900), La Plata, Argentina
[2]Institute for Bioengineering of Catalonia (IBEC), The Barcelona Institute of Science and Technology, 08028 Barcelona, Spain
[3]Instituto de Investigación Interdisciplinaria (I³), Vicerrectoría Académica, and Centro de Bioinformática, Simulación y Modelado (CBSM), Facultad de Ingeniería, Universidad de Talca, Campus Lircay, Talca 3460000, Chile
[4]Université de Lille, CNRS, INSERM, CHU Lille, Institut Pasteur de Lille, U1019-UMR9017, CIIL—Center for Infection and Immunity of Lille, F-59000 Lille, France
[5]CIBER-BBN, ISCIII, 08028 Barcelona, Spain
[6]Department of Materials Science and Physical Chemistry, University of Barcelona, 08028 Barcelona, Spain
[7]São Carlos Institute of Physics (IFSC-USP), University of São Paulo, 13566-590 São Carlos, São Paulo, Brazil
[8]Centro de Investigaciones en Química Biológica de Córdoba (CIQUIBIC), CONICET, Córdoba, Argentina
[9]Departamento de Química Biológica Raquel Caputto, Facultad de Cs. Químicas, Universidad Nacional de Córdoba. Haya de la Torre y Medina Allende, Ciudad Universitaria, Córdoba, Argentina
[10]These authors contributed equally
[11]Lead contact
*Correspondence: smate@med.unlp.edu.ar
https://doi.org/10.1016/j.isci.2024.110362

A

21-day-old male SHR rats

↓

Free fed for 16 weeks

Control group
(SHR; n=12)

Treated group
(SHR+ ω3; n=12)

ω3 FAs
supplementation

B

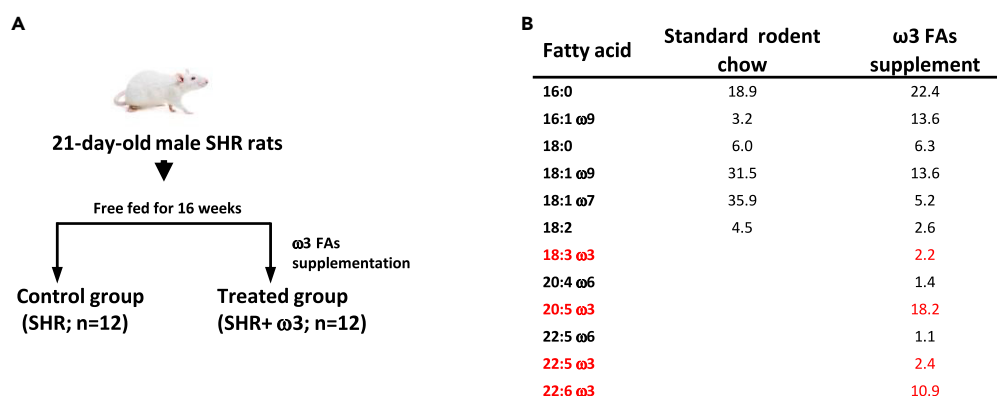| Fatty acid	Standard rodent chow	ω3 FAs supplement
16:0	18.9	22.4
16:1 ω9	3.2	13.6
18:0	6.0	6.3
18:1 ω9	31.5	13.6
18:1 ω7	35.9	5.2
18:2	4.5	2.6
18:3 ω3		2.2
20:4 ω6		1.4
20:5 ω3		18.2
22:5 ω6		1.1
22:5 ω3		2.4
22:6 ω3		10.9

Figure 1. Experimental design and FAs composition of the standard rodent chow diet and the ω3 FAs supplement
(A) SHR were separated into two groups, SHR control (SHR) and SHR treated (SHR+ ω3). Both groups were fed with standard rodent chow diet; the treated group received ω3 FAs orally every day during 16 weeks.
(B) Total FAs relative content of the standard rodent chow diet and the ω3 FAs supplement.

replicas of natural membranes—composed of hundreds to thousands of different lipid species and proteins—and may have limitations when capturing the full complexity and functionality of living systems.

The present work is aimed at expanding our understanding of the effects of ω3 FAs on the physicochemical properties of brain membranes. To perform these studies, we utilized a well-accepted animal model of essential hypertension, cognitive impairment, and dementia, the spontaneously hypertensive rats (SHR).[17] It has been shown that SHR have less polyunsaturated fatty acids, specifically DHA, in brain membranes when compared to the control strain Wistar Kyoto rats.[18] The approach relied on biochemical and biophysical measurements of (i) brain lipid membrane models, composed by cerebral cortex-total lipid extracts of SHR fed with a standard diet or a ω3 FAs-supplemented diet and (ii) synthetic lipid mixtures composed by commercial lipids, specifically phosphatidylcholine, sphingomyelin, and cholesterol (PC/SM/Chol) + DHA (free or esterified within phosphatidylcholine).

Membrane elasticity and phase separation were studied using Langmuir monolayers and Brewster angle microscopy (BAM); in addition, lipid-lipid interactions were explored by polarization modulation infrared reflection absorption spectroscopy (PM-IRRAS). Finally, the topography and nanomechanical properties of supported lipid bilayers (SLBs) were examined by atomic force microscopy (AFM)-force spectroscopy (FS). Our results revealed that ω3 FAs play a role in stabilizing lateral phase separation in the membranes. They achieve this by enhancing the physical differences between coexisting phases. These findings are significant as they contribute to a deeper understanding of the complexity of cellular membranes and how alterations in their lipid composition, such as an increase in ω3 FAs, can impact essential cellular processes.

RESULTS AND DISCUSSION

The experimental methodology and animal grouping utilized to investigate the impact of ω3 FAs supplementation on the physical properties of brain membranes are illustrated in Figure 1A. Panel B of the same figure demonstrates the FA composition of rodent feed and the dietary ω3 FAs supplement employed.

A significantly higher ω3 FAs content was detected in the plasma and cerebral cortex of hypertensive rats after dietary supplementation with ω3 FAs

After 16 weeks of daily administration of ω3 FAs to SHR, the plasma of the SHR+ ω3 group exhibited elevated levels of eicosapentaenoic acid, DHA and docosapentaenoic acid. This led to a significant increase in the overall content of ω3 FAs, as seen in panel A in Figure 2, from 2.7 ± 0.2 in SHR to 6.0 ± 0.5 in SHR+ ω3. We also found an increased proportion of total ω3 FAs detected in the cerebral cortex of SHR+ ω3 (9.4 ± 0.7), in comparison with SHR (7.7 ± 0.3) (Figure 2B). Note that the ratio of omega-6 to omega-3 FAs reduced significantly in both the plasma (5.2 ± 0.4) and cerebral cortex (1.6 ± 0.2) of SHR+ ω3, compared to the control group (18.1 ± 1.0) in plasma and (2.0 ± 0.1) in cerebral cortex (Figures 2C and 2D, respectively). These findings collectively demonstrate the effective incorporation of ω3 FAs into brain membranes through oral supplementation with physiologically relevant concentrations, initiated during the weaning period and sustained over four months.

The composition of overall FAs was analyzed in the cerebral cortex of SHR, with a particular focus on ω3 FAs. Therefore, we cannot determine whether they are present in their free or esterified form. Rapoport et al. demonstrated that the uptake of DHA in the brain occurs primarily from the free form of FA, which is produced by hydrolysis from plasma lipoproteins and transported bound to albumin.[19] Calculations of the kinetics of binding and unbinding of unesterified FAs to serum albumin indicate that approximately 5% of FA is released from albumin as blood passes through the brain.[20] Once it has entered the brain, unesterified DHA is largely (>80%) and selectively delivered via an acyl-CoA synthetase and acyltransferase to the stereospecific numbered sn-2 position of phospholipids. On the other hand, its precursors,
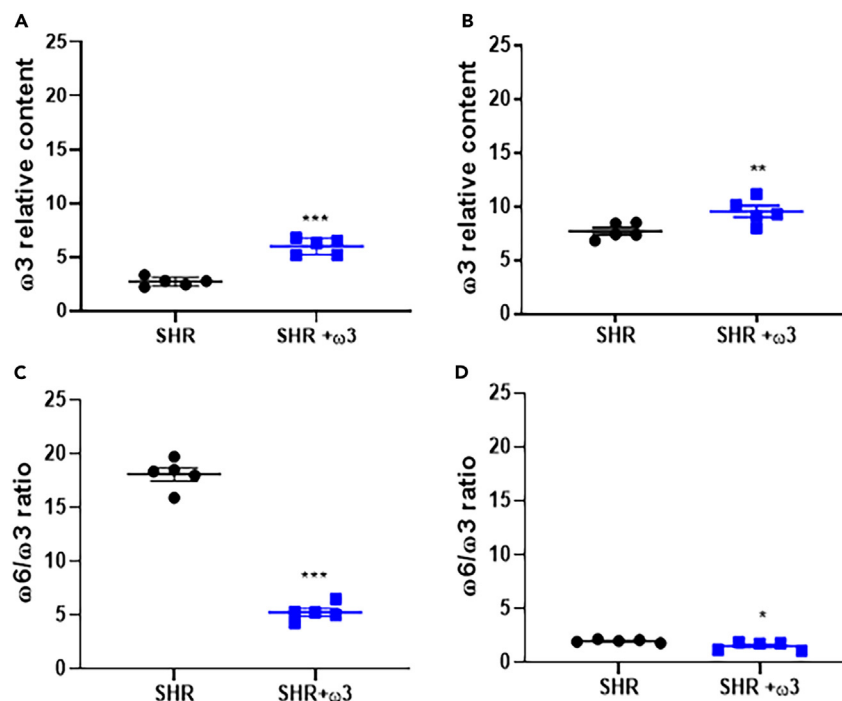
Figure 2. ω3 FAs supplementation increases the ω3 FAs total content and decreases ω6/ω3 ratio in plasma and cerebral cortex
ω3 FAs total content in plasma (A) and cerebral cortex (B). ω6/ω3 ratio in plasma (C) and cerebral cortex (D). Data are expressed as mean ± SEM (of percentage of total FAs). *indicates $p < 0.05$ vs. SHR; **indicates $p < 0.01$ vs. SHR, and ***indicates $p < 0.001$ vs. SHR, determined by Student's t test.

α-linolenic or eicosapentaenoic acid, are predominantly subjected to β-oxidation within mitochondria after transfer by carnitine acyltransferase from the brain's acyl-CoA pool.[21] These findings were considered when designing the experiments on synthetic lipid mixtures, as will be mentioned later on.

ω3 FAs supplementation enhances the elasticity of brain lipid monolayers

The impact of ω3 FA supplementation on the overall FA composition of the cerebral cortex led us to explore their biophysical implications. The experiments were conducted using lipid monolayers of total lipid extracts from the cerebral cortex of SHR+ ω3 or SHR. These are referred as brain lipid membranes.

The surface pressure-area isotherms in Figure 3A, show an expansion of SHR+ ω3 monolayers to higher areas per lipid content compared to SHR. Surface elasticity measurements evidenced a decrease in the Cs^{-1} values in SHR+ ω3, relative to SHR, indicative of a more elastic monolayer (Figure 3B). Cs^{-1} measured at 30 mN/m were 96 ± 4.8 mN/m for SHR and decreased to 76 ± 2.0 mN/m in SHR+ ω3. A lipid reorganization is observed at low surface pressures, which may reflect a phase transition from a liquid-expanded (Le) phase to a soft liquid-condensed phase (Lc). It occurs at higher surface pressures for SHR+ ω3 (7.0 ± 0.8 mN/m) than for SHR (5.0 ± 0.9 mN/m), evidencing a thermodynamic stabilization of the more expanded phase. This may be the consequence of a preferential partition of the ω3 lipids into the Le phase.[22]

ω3 FAs supplementation enhances phase disparity of brain lipid monolayers

The surface morphology analysis of brain lipid monolayers revealed phase coexistence in both SHR and SHR+ ω3 (Figures 4A and 4B, respectively). This is characterized by the presence of a thicker phase (light gray) forming circular domains immersed within a thinner phase (dark gray). Results by Pusterla et al.[23] for lipids extracted from purified myelin membranes of bovine spinal cord support the assignment of a liquid-ordered (Lo) character to the thick phase and a Le character to the thinner continuous phase. We then focused on the stability of observable membrane domains, quantified as the miscibility surface pressure. Phase coexistence persisted until a critical surface pressure was surpassed, approximately 7.8 ± 1 mN/m for SHR and 14.6 ± 1 mN/m for SHR+ ω3. Beyond this point—named miscibility surface pressure—both phases seamlessly merged. From Figure 2, one may infer that the incorporation of ω3 FAs into brain membranes leads to a reduction in lipid miscibility. This observation suggests a larger compositional gap between both phases, within the SHR+ ω3 group.[24] Consequently, the merging of these phases requires a higher degree of compression. The enhancement of phase separation by ω3 lipids is consistent with reports on the stabilization of B cells-raft *in vivo*, by diets rich in fish oil.[25,26] It should be said, on the other hand, that to the best of our knowledge, there have been no studies investigating the stability of membrane domains in the brain of the SHR animal model related to diet.
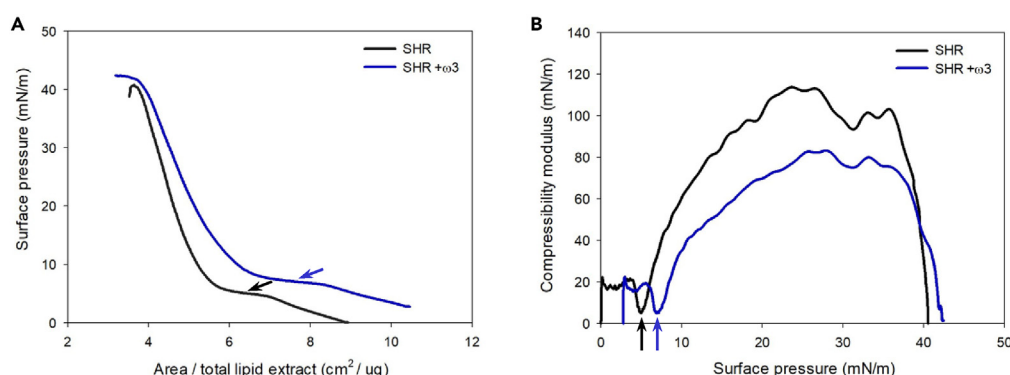
Figure 3. ω3 FAs supplementation enhances the elasticity of brain like lipid monolayers
(A) Surface-pressure-area isotherms.
(B) Compressibility moduli (C_s^{-1}) corresponding to each isotherm. Measurements were performed in Hepes-saline Buffer, pH 7.4, at 20 ± 1°C. Phase transitions are indicated with arrows in panels A and B.

Phase separation in model membranes has been related to the magnitude of the difference in physical properties between coexisting phases.[27,28] To investigate whether such an effect was responsible for the stabilization of Lo domains within the SHR+ ω3 group, we measured the average gray intensity for both phases in brain lipid monolayers. In SHR+ ω3, higher disparities in the average gray intensity values between phases were observed compared to SHR, spanning the entire range of surface pressures where phase separation was detected (Figures 4C and 4D, respectively). It should be recalled that the gray intensity in BAM experiments is influenced by both the refractive index and monolayer thickness.[23,24] Hence, the measurements suggest a greater distinction between lipid phases in the SHR+ ω3 group compared to the SHR group, reinforcing the conclusion of a larger compositional gap between phases. Larger differences in average gray intensity were recorded for the Le phases between SHR and SHR+ ω3 (27 at 5 mN/m and 11 at 7 mN/m) than for the Lo phases (7 at 5 mN/m and 5 at 7 mN/m)
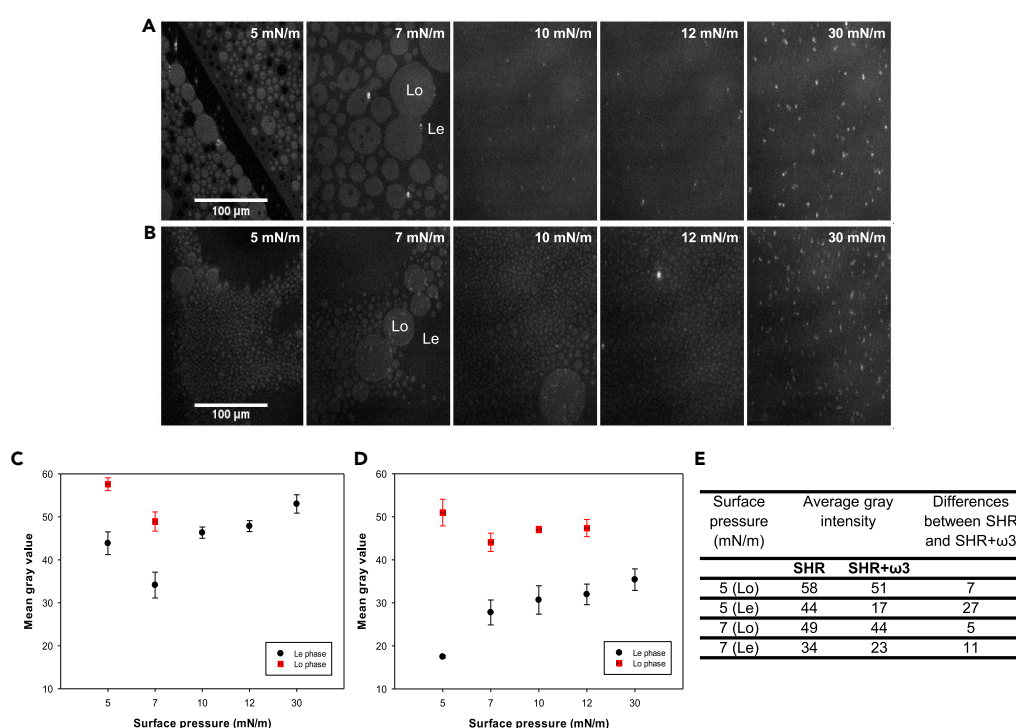

Figure 4. ω3 FAs supplementation enhances phase disparity of brain lipid monolayers
BAM images of brain lipid monolayers during compression in (A) SHR and (B) SHR+ ω3. Scale bar corresponds to 100 μm. All images were collected at 20°C and pH 7.4. Gray level measurements: (C) SHR or (D) SHR+ ω3. The red points indicate the gray level of the Lo and the black points of the Le phase. Data are represented as mean ± SEM. (E) Differences in average gray intensity values within Le or Lo phases between SHR and SHR+ ω3.

(Figure 4E). This larger effect on the Le phase and the small effect on the Lo phase in SHR+ ω3 suggest a model in which dietary ω3 FAs impact the properties of disordered phases[29] in cerebral cortex membranes. This contrasts with the alternative possibility that polyunsaturated lipids infiltrate and disrupt ordered domains.[30] However, we emphasize that we made no direct measurements of phases lipid composition, and thus our experiments could not distinguish between the specific mechanisms of enhanced phase separation. There was also a noteworthy reduction in the overall average gray intensity at 30 mN/m—a lateral pressure considered representative of the lipid packing in a cell membrane[31]—for SHR+ ω3 (35.4 $\pm$ 1) compared to SHR (53.0 $\pm$ 1). This is in line with the enhanced elasticity in Figure 3B, indicating a general disordering effect of ω3 FAs on brain lipid membranes.

ω3 FAs supplementation increases the differences in lipid packing between phases in brain SLBs, stabilizing membrane domains

The results obtained from BAM imaging suggested that ω3 FAs supplementation was responsible for enhancing the difference in physical properties between coexisting lipid phases in brain lipid monolayers. To further explore the impact of ω3 FAs supplementation on phase separation, we conducted AFM imaging and force spectroscopy measurements on SLBs, a model system that closely mimics the structure of natural cell membranes.[32] Experiments were performed on SLBs composed of cerebral cortex-total lipid extracts of SHR+ ω3 and SHR to assess their membrane topography and nanomechanical properties. Topographical images showed membrane patches with phase segregation in all samples (Figures 5A and 5D). In the SHR SLBs, three different phases were distinguished (Figure 5A): one with round-shaped thicker domains and two continuous-like phases. The three distinguishable phases show slightly different thickness. The height difference between them can be estimated from fitting the height distribution (Figure 5B), with Δh_{3-2} = 0.4 nm between the thicker and intermediate phase, Δh_{2-1} = 0.8 nm between the intermediate and thinner phases, and therefore Δh_{1-3} = 1.2 nm between the thinner and thicker phases. Although not many topographical studies can be found on lipid bilayers built from cerebral cortex-total lipid extracts, SLBs obtained from naked mole-rat brain lipid extracts[33] have been shown to have a two-tier raft structure, similar to what we observe for SHR SLBs. For the SHR+ ω3 we found SLBs also segregated in three different phases (Figure 5D), however, the thicker domains are extense, more heterogeneous, and less round in shape. We also distinguish a continuous phase and small irregular domains present in this continuous phase. The height analysis gives a distribution that can be deconvoluted into 3 contributions (Figure 5E). This allows an estimation of the difference in thickness between the coexisting phases to be Δh_{3-2} = 0.3 nm between the thicker and intermediate phases and Δh_{2-1} = 0.3 nm between the intermediate domains and thinner phase, and therefore a difference in thickness between the thicker and thinner phases of Δh_{1-3} = 0.6 nm. Although it can be observed qualitatively that the difference in phase heights is slightly smaller in the SHR +ω3 than in the SRH case, the most remarkable fact is the coexistence of three phases with a prevailing proportion of a phase with intermediate thickness in SHR, whereas this phase tends to disappear in the SHR +ω3, that show less amount of this intermediate phase and a higher proportion of the thicker and thinner phases.

We then performed force-separation curves on previously imaged areas by approaching and retracting the AFM probe at constant velocity in a force map mode. By applying vertical load at constant velocity, we can assess the force at which the membrane is pierced by the AFM probe, i.e., the breakthrough force (F_b).[34] Therefore, F_b maps and adhesion force maps can be built to relate the membrane mechanical properties with the different domain structures in the topographical images. After the membrane has been pierced by the AFM probe, sometimes adhesion between the probe and the bilayer is reflected as deflection toward the sample at the contact point. This allows one to calculate the adhesion force. The adhesion maps (Figures 6C and 6D) show that the higher and lower adhesion forces correspond to the thicker and thinner domains, respectively. The contrast in adhesion relates to the different compositions.[35] The different phases exhibit diverse mechanical properties, with the thicker one being the most resilient (higher F_b, Figures 6E–6I). For SHR SLBs, although F_b maps (Figure 6E) show a correlation with the different phases observed in topography, the sampling of our experiments leads to a unimodal distribution with an average value of 1.9 $\pm$ 0.5 nN (Figure 6G), although higher forces are seen for the small round thicker domains. For the SHR+ ω3 SLBs, however, a bimodal distribution of F_b is obtained with average values of 0.9 $\pm$ 0.4 and 4.4 $\pm$ 0.5 nN (Figure 6H), suggesting an increase in the lipid packing disparity between the coexisting phases, and a decrease of the presence of an intermediate phase. This is also reflected in the F_b map (Figure 6F). In all cases, higher forces correspond to thicker domains and lower forces to the thinner ones.

In summary, brain SLBs of SHR and SHR+ ω3 show a phase-segregated topography, but the coexisting phases in SHR+ ω3 are nanomechanically more different among them (Figure 6I). These findings align with the average gray intensity values in cerebral brain lipid monolayers (see Figures 4C and 4D). Since F_b depends strongly on the bilayer chemical composition,[36] one may infer that dietary ω3 FAs incorporated into the brain's plasma membranes in SHR+ ω3 enhance the difference in lipid packing between the coexisting phases.

Free DHA and DHA esterified within phosphatidylcholine enhance the elasticity of Langmuir monolayers in synthetic lipid mixtures

Our findings regarding brain lipid membranes of SHR, which contain hundreds to thousands of different lipid species, indicate that dietary ω3 FAs integrated into the plasma membranes of the brain, enhancing their elasticity and leading to an increased lipid phase disparity. However, the lipid complexity of these model systems and the myriad of potential cellular outcomes linked to feeding SHR with ω3 FAs make it challenging to attribute our findings to the impact of incorporating ω3 FAs into membrane lipids. To examine the relationship between ω3 FAs and phase separation directly, we delved into phase coexistence and lipid packing in well-defined synthetic lipid mixtures. We conducted experiments using monolayers of a standard raft mixture consisting of PC, SM, and Chol[37,38] in the presence of both free DHA and DHA esterified within phosphatidylcholine (SDPC). We assayed both forms of DHA, free and SDPC, to gather insights that could apply to the conditions
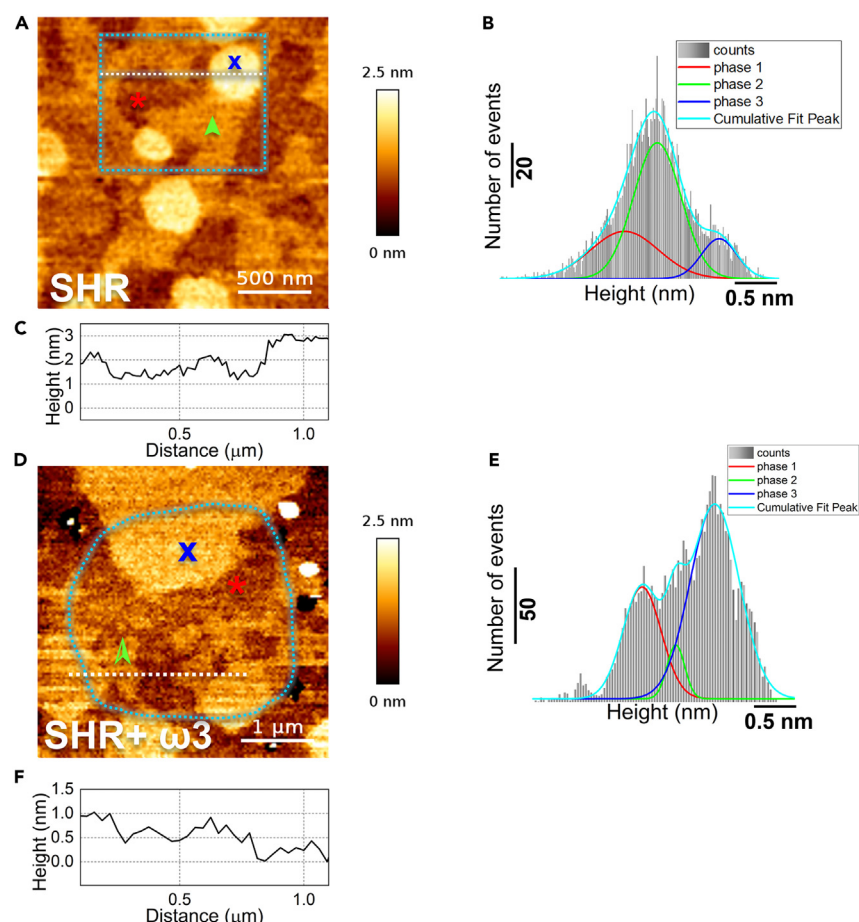
Figure 5. ω3 FAs supplementation changes the phase segregation patterns detected in AFM

AFM topography height analysis of brain SLBs composed of cerebral cortex-total lipid extracts of SHR and SHR+ ω3.

(A) AFM topography image of SLB formed by SHR lipid extracts, where 3 different phases of different height are discernable. Scale bar corresponds to 500 nm.

(B) Histogram representing the number of events versus the measured height of the pixel values of the blue box in (A). Light blue shows the fitting corresponding to all pixels in the blue box in (A). Red shows the Gaussian fitting for the values of the lowest phase—phase 1—marked in (A) by a red star. Green shows the Gaussian fitting corresponding to the intermediate height phase—phase 2—marked in (A) by a green arrowhead. Dark blue shows the Gaussian fitting for the highest height phase—phase 3—marked in (A) by a dark blue cross.

(C) Section profile of the white dotted line drawn in (A).

(D) AFM topography image of SLB formed by SHR+ ω3 lipid extracts, where 3 different phases of different height are discernable. Scale bar corresponds to 1 μm.

(E) Histogram representing the number of events versus the measured height of the pixel values in the region delimited by the blue dotted line in (D). Light blue shows the fitting for all pixels in the region delimited by the blue dotted line in (D). Red shows the Gaussian fitting of the values of the lowest phase—phase 1—marked in (D) by a red star. Green shows the Gaussian fitting corresponding to the intermediate height phase—phase 2—marked in (D) by a green arrowhead. Dark blue shows the Gaussian fitting for the highest height phase—phase 3—marked in (D) by a dark blue cross.

(F) Section profile corresponding to the white dotted line drawn in (D).

found in brain plasma membranes of SHR+ ω3. Dietary ω3 FAs are primarily esterified within membrane PC and phosphatidylethanolamine. However, there are circumstances, such as during FAs uptake or under conditions where a phospholipase A_2 is activated, in which a temporary and localized increase in the free FA form can occur.[15]

The surface pressure-area isotherms in Figure 7A, show an expansion of the monolayers to higher areas when the ω3 lipids were incorporated at 10-mole percent into the PC/SM/Chol mixture. In free DHA-containing films, the increase in molecular area occurred only at low surface pressures, while the addition of SDPC produced larger increments along the whole isotherm until monolayer collapse. This was expected from the higher mean molecular area of the PC phospholipid compared to the free FA. The SDPC-containing films collapsed at lateral pressures of 42.5 ± 1.0 mN/m, similar to the PC/SM/Chol monolayers, which collapsed at 43.3 ± 1.0 mN/m. In contrast, with DHA, the collapse surface pressure decreased to 39.0 ± 0.8 mN/m, pointing to less stable monolayers in the presence of free FA. A decrease in Cs^{-1} was observed for mixtures with DHA or SDPC (Figure 7B), indicative of more compressible monolayers in the presence of either lipid. Cs^{-1} measured at the biological relevant surface pressure of 30 mN/m were 90.0 ± 6.0 mN/m for the ternary lipid films, and 64.3 ± 0.7 mN/m
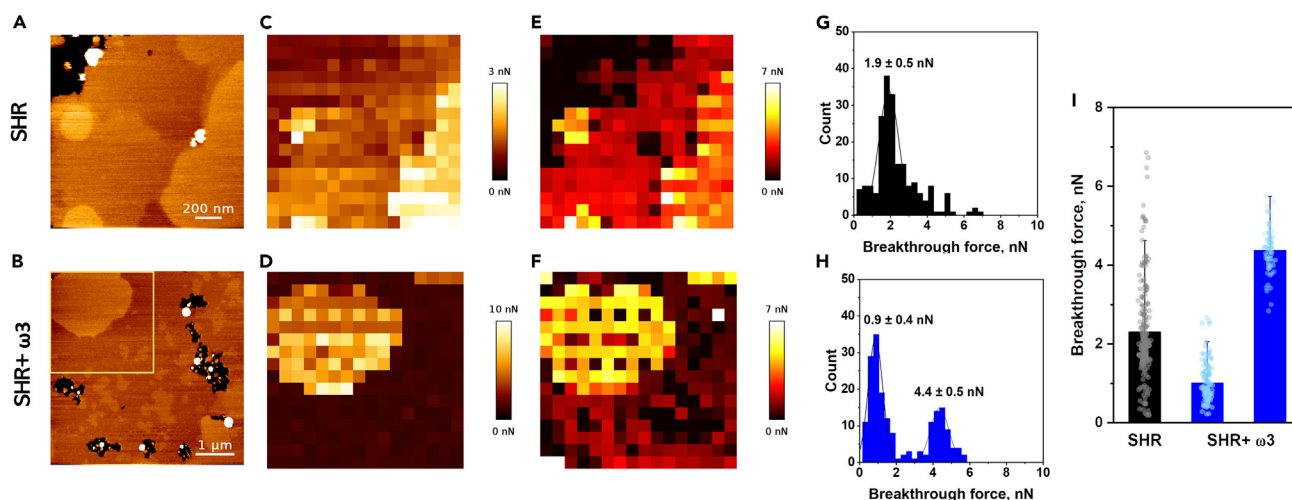
Figure 6. ω3 FAs supplementation increases lipid packing disparity between phases in brain SLBs, stabilizing membrane domains

AFM topography and nanomechanical analysis of SLBs from cerebral cortex-total lipid extracts of SHR and SHR+ ω3. Topographical images of SLBs from SHR (A) and SHR+ ω3 (B); adhesion maps of SLBs from SHR (C) and SHR+ ω3 (D); breakthrough force maps of SLBs from SHR (E) and SHR+ ω3 (F) and breakthrough force distributions of SLBs from SHR (G) and SHR+ ω3 (H), from representative samples. (I) Breakthrough force statistical analysis of all samples measured (average ±SD, n between 185 and 200). All measurements were done at room temperature and in 150 mM NaCl, 25 mM HEPES buffer, pH 7.6. Scale bar for Figure in A corresponds to 200 nm. C and E are maps on the same area as Figure in A. Scale bar for Figure in B corresponds to 1 μm. D and F correspond to maps in the 3 × 3 μm² area marked of B.

and 60.7 ± 5.2 mN/m in monolayers containing 10% of DHA and SDPC, respectively. In brief, free and esterified DHA expanded and enhanced the elasticity of Langmuir monolayers in these synthetic lipid mixtures.

Free DHA and DHA esterified within phosphatidylcholine reduce molecular packing of Langmuir monolayers in synthetic lipid mixtures

The PM-IRRAS technique was applied to monitor the vibrational spectra of ternary lipid films at 30 mN/m in the presence of DHA or SDPC (Figures 8A–8C). This technique is useful for studying lipid-lipid interactions, providing detailed information about the lipid molecules' orientation, ordering, and conformation at the interface. It may detect changes not only in the hydrocarbon chains but also in the polar headgroups of the lipids.[39] In line with a previous report,[40] the CH region of PC/SM/Chol monolayers had main bands at 2920 and 2851 cm^{-1} assigned to CH$_2$ asymmetric and symmetric stretching vibrations, respectively (Figure 8A). The spectra of the ternary mixture with 10% of ω3 polyunsaturated lipids show the CH$_2$ bands at similar wavenumbers, while bands assigned to the asymmetric stretching of CH$_3$ groups also appeared. The presence of CH$_3$ bands—absent in the ternary lipid film—indicates a higher conformational disorder in the acyl chains region when DHA or SDPC were incorporated into the ternary lipid mixture.[41,42]

The 1800–1600 cm^{-1} region of the PM-IRRAS spectra provides information on the C=O stretching modes of ester (PC) and amide groups (SM amide I band).[43] In PC/SM/Chol films, the spectra had an intense band at 1740 cm^{-1} assigned to C=O stretching mode of PC and an asymmetric amide I band at 1678 cm^{-1} assigned to non- or weakly H-bonded amide groups and a second component at 1650 cm^{-1} assigned to H-bonded groups (Figure 8B). The addition of DHA inverted the relative intensity of the high-frequency-to-low-frequency components of the amide I band, which appeared red-shifted to 1686 and 1670 cm^{-1}, suggesting a weaker H-bonding network of SM. Also, a broadened C=O band was detected which shifted its maximum to 1752 cm^{-1} with a second component at 1720 cm^{-1}. The latter wavenumbers revealed more dehydrated and hydrated C=O groups, respectively, in these monolayers. In mixtures with SDPC, a broader C=O band was also observed, blue-shifted to 1736 cm^{-1}, indicative of higher levels of hydration of the ester groups of PC. The amide I band maintained the shape of the ternary lipid mixture, although shifted to lower wavenumbers. This shift can be considered indicative of stronger H-bonded SM in the films containing ω3 SDPC.[44]

The phosphate region between 1300 and 1000 cm^{-1} was also analyzed in Figure 8C. Together with C=O, PO$_2^-$ stretching modes are sensitive to the lipid environment and respond to changes in hydration and H-bonding.[45] In the ternary lipid mixture, two well-defined bands were detected at 1253 and 1215 cm^{-1} for the PO$_2^-$ asymmetric stretching mode corresponding to dehydrated and hydrated PO$_2^-$ groups, respectively.[43,46] The symmetric PO$_2^-$ stretching bands appeared at 1126 and 1085 cm^{-1} while the diester phosphate (C–O–P–O–C) stretching band at 1057 cm^{-1}. A band at 1161 cm^{-1} could be assigned to the ester C-O asymmetric stretching of PC.[47] In the presence of DHA, the shape of the asymmetric PO$_2^-$ bands changed drastically to a broad one encompassing the two distributions observed in the ternary films, with a maximum at 1230 cm^{-1}. The latter result reflects a more heterogeneous level of hydration of the PO$_2^-$ groups compared to the ternary lipid system. One main band assigned to the PO$_2^-$ symmetric stretching appeared at 1107 cm^{-1} while the C–O–P–O–C stretching band increased in intensity and shifted to lower wavenumbers (1041 cm^{-1}) owing to changes in the orientation of phospholipid headgroups in
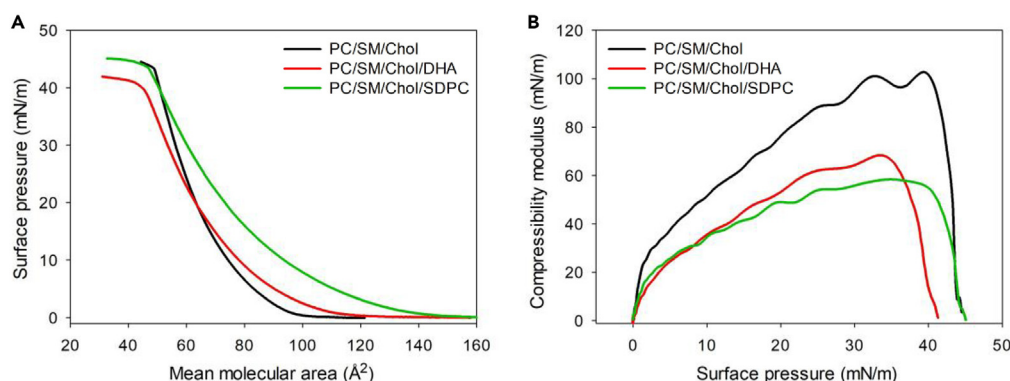
Figure 7. Free and esterified DHA enhance the elasticity of Langmuir monolayers

(A) Surface pressure-area isotherms of the lipid mixtures PC/SM/Chol (2:1:1), PC/SM/Chol/DHA, and PC/SM/Chol/SDPC (2:1:1 ternary mixture +10-mole percent of DHA or SDPC).

(B) Compressibility moduli (C_s^{-1}) corresponding to each isotherm. Measurements were performed in Hepes-saline Buffer, pH 7.4, at 20 ± 1°C.

the presence of free DHA.[48] In SDPC-containing films, the PO_2^- asymmetric stretching mode had one main band at lower wavenumbers (1222 cm^{-1}) than the ternary lipid films, pointing to a higher hydration level in the interfacial region. The phosphate diester band also increased and appeared at lower wavenumbers (1049 cm^{-1}) than in the ternary mixture, as observed in monolayers with free DHA. Hence, the orientation of the phospholipids headgroups changes in the presence of SDPC.

In summary, PM-IRRAS measurements in synthetic lipid mixtures allowed the direct characterization of the major chemical groups in the lipid films and confirmed the disordering effect of DHA that was inferred from Langmuir monolayers (Figures 3 and 4) and SLBs (Figures 5 and 6) on brain lipid membranes. In agreement with the inferences from those experiments, the PM-IRRAS observations demonstrated a decrease in lipid packing within mixtures of canonical rafts when they contained DHA. This occurred regardless of whether DHA was in its free form or as an esterified compound, pointing to the *cis*-double bonds of these ω3 polyunsaturated lipids as the main responsible for this effect. Incorporating ω3 lipids also affected the interfacial region, increasing the hydration levels of the polar headgroups and inducing
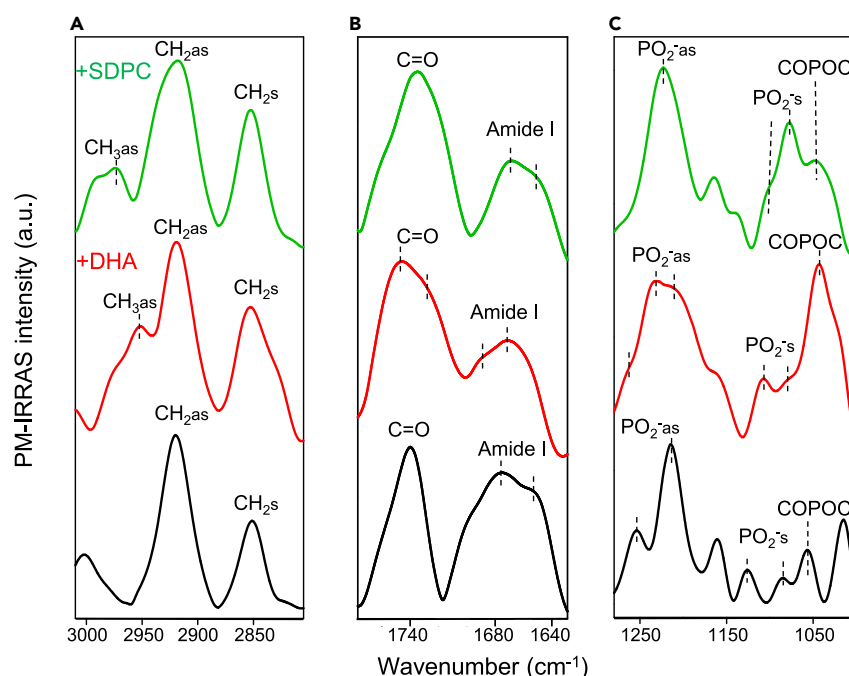

Figure 8. Free DHA and SDPC reduce molecular packing of ternary lipid mixtures, alter the H-bonding network, and increase the hydration levels of the headgroups in Langmuir monolayers

Hydrocarbon chains (A), carbonyl (B), and phosphate (C) regions of the PM-IRRAS spectra of monolayers of PC/SM/Chol (black trace), PC/SM/Chol/DHA (red trace), and PC/SM/Chol/SDPC (green trace) at a lateral pressure of 30 mN/m. Measurements were performed in Hepes-saline buffer, pH 7.4, at 20 ± 1°C.

changes in the orientation of the phospholipids headgroups. On the other hand, the incorporation of free or esterified DHA modified the SM H-bonding patterns; free DHA-containing monolayers presented weaker SM H-bonding networks, while stronger H-bonded SM species were detected in SDPC–containing films. PM-IRRAS thus allowed us to discriminate the effects of both lipids on the overall behavior of the mono-layer's chemical groups at the interface.

Our research aligns with compelling investigations indicating a fundamental mechanism through which dietary fats influence cellular phys-iology by reshaping membrane lipidomes and altering biophysical characteristics, including phase disparity.[49,50] In this concern, it is worth noticing that Levental et al. have recently proposed a mammalian mechanism for maintaining membrane homeostasis, wherein lipidome re-modeling in response to dietary lipid inputs preserves functional membrane phenotypes.[51] Their study demonstrated that exogenous poly-unsaturated fatty acids are incorporated into membrane lipids, leading to a decrease in membrane packing. This reduction is rapidly compen-sated both *in vitro* and *in vivo* by extensive lipidome remodeling, most notably through the upregulation of saturated lipids and Chol, thereby restoring membrane packing and permeability. In this study, we orally supplemented rats under pathological conditions (SHR; model of essential hypertension, cognitive impairment, and dementia) that show decreased basal levels of polyunsaturated fatty acids, especially DHA.[18] In this scenario, we found that 16 weeks of ω3 supplementation led to a significant change in the ω3 FA composition compared to non-treated animals, along with changes in the physical properties of whole-cell membrane lipids extracted from their brain cortex. These findings strongly encourage further research into the mechanisms that regulate membrane lipid dynamics in response to dietary changes, including their temporal aspects and interactions across different tissues in normal and pathological conditions.

Conclusion

Neurodegenerative disorders manifest through a gradual deterioration of the central nervous system, marked by ongoing neuronal damage and loss. Despite significant research efforts, effective therapeutic interventions are still lacking which can modify the course of neurodegen-erative diseases. Identifying the pivotal molecular-level structural changes essential to the initiation and advancement of these diseases proves to be a complex task. Within this framework, the physicochemical properties of brain cell membranes are believed to be modulated by ω3 FAs, potentially impacting cell functions and, in turn, overall brain health. This study supports this idea, evidencing that dietary supple-mentation with ω3 FAs affects the physicochemical behavior of rat-brain lipids, at the molecular and nanoscale levels. Our findings indicate a significant elevation in ω3 levels in the cerebral cortex of SHR+ ω3. Moreover, it induced alterations in the physical properties of monolayers and bilayers made from brain lipids, including changes in molecular packing, elasticity, and lipid miscibility, resulting in an increased phase disparity. Upon employing PM-IRRAS, we verified that both free and esterified DHA reduced the molecular packing of hydrocarbon chains, altered the H-bonding network, and increased hydration levels of headgroups in synthetic lipid mixtures, thus enhancing phase separation. These alterations in the physicochemical properties of rat-brain lipids induced by ω3 FAs could impact brain functions and cognition. In forth-coming research, we aim to provide insights into how the content of ω3 FAs and the physicochemical features of rat-brain membranes influ-ence the cognitive and behavioral aspects of rats.

Limitations of the study

It is important to emphasize the significant differences between plasma membranes within living cells and the brain-like membrane systems that are the focus of our investigation, made of total lipids extracted from rat-brain cortices. These disparities encompass the disruption of precise membrane asymmetry and a widespread reduction in the presence of membrane proteins. While the exact ramifications of these dis-tinctions on the physicochemical attributes of membranes remain unresolved, it is worth underscoring that our brain-like membrane systems present a valuable experimental paradigm for elucidating the biophysical traits inherent in membranes possessing the intricate lipid complexity and composition characteristic of biological systems.

STAR★METHODS

Detailed methods are provided in the online version of this paper and include the following:

- KEY RESOURCES TABLE
- RESOURCE AVAILABILITY
  - Lead contact
  - Materials availability
  - Data and code availability
- EXPERIMENTAL MODEL AND STUDY PARTICIPANT DETAILS
- METHOD DETAILS
  - Materials
  - Animals and treatment
  - Blood collection and cerebral cortex isolation
  - Fatty acid analysis
  - Surface pressure- area isotherms
  - Brewster Angle Microscopy (BAM)
  - Polarization Modulation Infrared Reflection Absorption Spectroscopy (PM-IRRAS) experiments

    ○ AFM imaging and force spectroscopy measurements
- QUANTIFICATION AND STATISTICAL ANALYSIS

AUTHOR CONTRIBUTIONS

Conceptualization, S.M.M.; methodology, M.I.G., L.R.-M., M.L.F., O.N.O. Jr., and S.M.M.; investigation, M.L.L., R.F.V., M.J.B., M.I.G., L.R.-M., and R.A.Z.; writing – original draft, S.M.M.; writing –review & editing, R.F.V., M.I.G., L.R.-M., O.N.O. Jr., and S.M.M.; funding acquisition, R.F.V., and S.M.M.; resources, M.L.F., M.I.G., L.R.-M., and O.N.O. Jr.; supervision, S.M.M.; project administration, S.M.M.

DECLARATION OF INTERESTS

The authors declare no competing interests.

DECLARATION OF GENERATIVE AI AND AI-ASSISTED TECHNOLOGIES IN THE WRITING PROCESS

During the preparation of this work the author used *Open AI Service* in order to improve language and readability. After using this *Tool/Service*, the author(s) reviewed and edited the content as needed and take(s) full responsibility for the content of the publication.

REFERENCES

1. Florent-Béchard, S., Malaplate-Armand, C., Koziel, V., Kriem, B., Olivier, J.L., Pillot, T., and Oster, T. (2007). Towards a nutritional approach for prevention of Alzheimer's disease: biochemical and cellular aspects. J. Neurol. Sci. 262, 27–36. https://doi.org/10.1016/j.jns.2007.06.046.

2. Kulzow, N., Witte, A.V., Kerti, L., Grittner, U., Schuchardt, J.P., Hahn, A., and Floel, A. (2016). Impact of Omega-3 fatty acid supplementation on memory functions in healthy older adults. J. Alzheimers Dis. 51, 713–725. https://doi.org/10.1016/j.biopsycho.2011.10.006.

3. Ichinose, T., Matsuzaki, K., Kato, M., Tanabe, Y., Tachibana, N., Morikawa, M., Kato, S., Ohata, S., Ohno, M., Wakatsuki, H., et al. (2021). Intake of docosahexaenoic acid-enriched milk beverage prevents age-related cognitive decline and decreases serum bone resorption marker levels. J. Oleo Sci. 70, 1829–1838. https://doi.org/10.5650/jos.ess21195.

4. Yamagata, K. (2023). Docosahexaenoic acid inhibits ischemic stroke to reduce vascular dementia and Alzheimer's disease. Prostaglandins Other Lipid Mediat. 167, 106733. https://doi.org/10.1016/j.prostaglandins.2023.106733.

5. Kim, H.Y. (2007). Novel metabolism of docosahexaenoic acid in neural cells. J. Biol. Chem. 282, 18661–18665. https://doi.org/10.1074/jbc.R700015200.

6. Zhang, W., Liu, J., Hu, X., Li, P., Leak, R.K., Gao, Y., and Chen, J. (2015). n-3 Polyunsaturated fatty acids reduce neonatal hypoxic/ischemic brain injury by promoting phosphatidylserine formation and Akt signaling. Stroke 46, 2943–2950. https://doi.org/10.1161/STROKEAHA.115.010815.

7. Kim, H.Y., Akbar, M., and Lau, A. (2003). Effects of docosapentaenoic acid on neuronal apoptosis. Lipids 38, 453–457. https://doi.org/10.1007/s11745-003-1083-z.

8. Serhan, C.N. (2017). Treating inflammation and infection in the 21st century: new hints from decoding resolution mediators and mechanisms. FASEB J. 31, 1273–1288. https://doi.org/10.1096/fj.201601222R.

9. Miyazawa, K., Fukunaga, H., Tatewaki, Y., Takano, Y., Yamamoto, S., Mutoh, T., and Taki, Y. (2020). Alzheimer's disease and specialized pro-resolving lipid mediators: Do MaR1, RvD1, and NPD1 show promise for prevention and treatment? Int. J. Mol. Sci. 21, 5783. https://doi.org/10.3390/ijms21165783.

10. Escribá, P.V., Busquets, X., Inokuchi, J.i., Balogh, G., Török, Z., Horváth, I., Harwood, J.L., and Vígh, L. (2015). Membrane lipid therapy: Modulation of the cell membrane composition and structure as a molecular base for drug discovery and new disease treatment. Prog. Lipid Res. 59, 38–53. https://doi.org/10.1016/j.plipres.2015.04.003.

11. Huber, T., Rajamoorthi, K., Kurze, V.F., Beyer, K., and Brown, M.F. (2002). Structure of Docosahexaenoic Acid-Containing Phospholipid Bilayers as Studied by 2 H Nmr and Molecular Dynamics Simulations. J. Am. Chem. Soc. 124, 298–309. https://doi.org/10.1021/ja011383j.

12. Shaikh, S.R. (2012). Biophysical and biochemical mechanisms by which dietary N-3 polyunsaturated fatty acids from fish oil disrupt membrane lipid rafts. J. Nutr. Biochem. 23, 101–105. https://doi.org/10.1016/j.jnutbio.2011.07.001.

13. Levental, K.R., Lorent, J.H., Lin, X., Skinkle, A.D., Surma, M.A., Stockenbojer, E.A., Gorfe, A.A., and Levental, I. (2016). Polyunsaturated Lipids Regulate Membrane Domain Stability by Tuning Membrane Order. Biophys. J. *110*, 1800–1810. https://doi.org/10.1016/j.bpj.2016.03.012.

14. Hishikawa, D., Valentine, W.J., Iizuka-Hishikawa, Y., Shindou, H., and Shimizu, T. (2017). Metabolism and functions of docosahexaenoic acid-containing membrane glycerophospholipids. FEBS Lett. *591*, 2730–2744. https://doi.org/10.1002/1873-3468.12825.

15. De Santis, A., Varela, y., Sot, J., D'Errico, G., Goñi, F.M., and Alonso, A. (2018). Omega-3 polyunsaturated fatty acids do not fluidify bilayers in the liquid-crystalline state. Sci. Rep. *8*, 16240. https://doi.org/10.1038/s41598-018-34264-3.

16. Li, X., Zhou, S., and Lin, X. (2022). Molecular View on the Impact of DHA Molecules on the Physical Properties of a Model Cell Membrane. J. Chem. Inf. Model. *62*, 2421–2431. https://doi.org/10.1021/acs.jcim.2c00074.

17. Amenta, F., Di Tullio, M.A., and Tomassoni, D. (2003). Arterial hypertension and brain damage-evidence from animal models (review). Clin. Exp. Hypertens. *25*, 359–380. https://doi.org/10.1081/ceh-120023545.

18. Liso Navarro, A.A., Sikoglu, E.M., Heinze, C.R., Rogan, R.C., Russell, V.A., King, J.A., and Moore, C.M. (2014). Effect of diet on brain metabolites and behavior in spontaneously hypertensive rats. Behav. Brain Res. *270*, 240–247. https://doi.org/10.1016/j.bbr.2014.05.013.

19. Rapoport, S.I., Ramadan, E., and Basselin, M. (2011). Docosahexaenoic Acid (DHA) Incorporation into the Brain from Plasma, as an In Vivo Biomarker of Brain DHA Metabolism and Neurotransmission. Prostaglandins Other Lipid Mediat. *96*, 109–113. https://doi.org/10.1016/j.prostaglandins.2011.06.003.

20. Smith, Q.R., and Nagura, H. (2001). Fatty acid uptake and incorporation in brain: studies with the perfusion model. J. Mol. Neurosci. *16*, 167–221. https://doi.org/10.1385/JMN:16:2-3:167.

21. Chen, C.T., Liu, Z., and Bazinet, R.P. (2011). Rapid de-esterification and loss of eicosapentaenoic acid from rat brain phospholipids: an intracerebroventricular study. J. Neurochem. *116*, 363–373. https://doi.org/10.1111/j.1471-4159.2010.07116.x.

22. Fanani, M.L., and Wilke, N. (2018). Regulation of phase boundaries and phase-segregated patterns in model membranes. Biochim. Biophys. Acta. Biomembr. *1860*, 1972–1984. https://doi.org/10.1016/j.bbamem.2018.02.023.

23. Pusterla, J.M., Cannas, S.A., Schneck, E., and Oliveira, R.G. (2022). Purified myelin lipids display a critical mixing point at low surface pressure. Biochim. Biophys. Acta. Biomembr. *1864*, 183874. https://doi.org/10.1016/j.bbamem.2022.183874.

24. Fanani, M.L., and Maggio, B. (2011). Liquid-liquid domain miscibility driven by composition and domain thickness mismatch in ternary lipid monolayers. J. Phys. Chem. B *115*, 41–49. https://doi.org/10.1021/jp107344t.

25. Rockett, B.D., Teague, H., Harris, M., Melton, M., Williams, J., Wassall, S.R., and Shaikh, S.R. (2012). Fish oil increases raft size and membrane order of B cells accompanied by differential effects on function. J. Lipid Res. *53*, 674–685. https://doi.org/10.1194/jlr.M021782.

26. Teague, H., Harris, M., Fenton, J., Lallemand, P., Shewchuk, B.M., and Shaikh, S.R. (2014). Eicosapentaenoic and docosahexaenoic acid ethyl esters differentially enhance B-cell activity in murine obesity. J. Lipid Res. *55*, 1420–1433. https://doi.org/10.1194/jlr.M049809.

27. Levental, I., Grzybek, M., and Simons, K. (2011). Raft domains of variable properties and compositions in plasma membrane vesicles. Proc. Natl. Acad. Sci. USA *108*, 11411–11416. https://doi.org/10.1073/pnas.1105996108.

28. Sezgin, E., Gutmann, T., Buhl, T., Dirkx, R., Grzybek, M., Coskun, Ü., Solimena, M., Simons, K., Levental, I., and Schwille, P. (2015). Adaptive lipid packing and bioactivity in membrane domains. PLoS One *10*, e0123930. https://doi.org/10.1371/journal.pone.0123930. eCollection 2015.

29. Shaikh, S.R., Kinnun, J.J., Leng, X., Williams, J.A., and Wassall, S.R. (2015). How polyunsaturated fatty acids modify molecular organization in membranes: insight from NMR studies of model systems. Biochim. Biophys. Acta *1848*, 211–219. https://doi.org/10.1016/j.bbamem.2014.04.020.

30. Williams, J.A., Batten, S.E., Harris, M., Rockett, B.D., Shaikh, S.R., Stillwell, W., and Wassall, S.R. (2012). Docosahexaenoic and eicosapentaenoic acids segregate differently between raft and nonraft domains. Biophys. J. *103*, 228–237. https://doi.org/10.1016/j.bpj.2012.06.016.

31. Marsh, D. (1996). Lateral pressure in membranes. Biochim. Biophys. Acta *1286*, 183–223. https://doi.org/10.1016/s0304-4157(96)00009-3.

32. Redondo-Morata, L., Losada-Pérez, P., and Giannotti, M.I. (2020). Lipid bilayers: Phase behavior and nanomechanics. Curr. Top. Membr. *86*, 1–55. https://doi.org/10.1016/bs.ctm.2020.08.005.

33. Frankel, D., Davies, M., Bhushan, B., Kulaberoglu, Y., Urriola-Munoz, P., Bertrand-Michel, J., Pergande, M.R., Smith, A.A., Preet, S., Park, T.J., et al. (2020). Cholesterol-rich naked mole-rat brain lipid membranes are susceptible to amyloid beta-induced damage in vitro. Aging *12*, 22266–22290. https://doi.org/10.18632/aging.202138.

34. Gumí-Audenis, B., Costa, L., Carlà, F., Comin, F., Sanz, F., and Giannotti, M.I. (2016). Review. Structure and Nanomechanics of Model Membranes by Atomic Force Microscopy and Spectroscopy: Insights into the Role of Cholesterol and Sphingolipids. Membranes *6*, 1–19. https://doi.org/10.3390/membranes6040058.

35. Picas, L., Suárez-Germà, C., Teresa Montero, M., and Hernández-Borrell, J. (2010). Force Spectroscopy Study of Langmuir−Blodgett Asymmetric Bilayers of Phosphatidylethanolamine and Phosphatidylglycerol. J. Phys. Chem. B *114*, 3543–3549. https://doi.org/10.1021/jp910882e.

36. Garcia-Manyes, S., Redondo-Morata, L., Oncins, G., and Sanz, F. (2010). Nanomechanics of lipid bilayers: heads or tails? J. Am. Chem. Soc. *132*, 12874–12886. https://doi.org/10.1021/ja1002185.

37. Maté, S., Busto, J.V., García-Arribas, A.B., Sot, J., Vazquez, R., Herlax, V., Wolf, C., Bakás, L., and Goñi, F.M. (2014). N-nervonoylsphingomyelin (C24:1) prevents lateral heterogeneity in cholesterol-containing membranes. Biophys. J. *106*, 2606–2616. https://doi.org/10.1016/j.bpj.2014.04.054.

38. Vázquez, R.F., Ovalle-García, E., Antillón, A., Ortega-Blake, I., Bakás, L.S., Muñoz-Garay, C., and Maté, S.M. (2021). Asymmetric bilayers mimicking membrane rafts prepared by lipid exchange: Nanoscale characterization using AFM-Force spectroscopy. Biochim. Biophys. Acta. Biomembr. *1863*, 183467. https://doi.org/10.1016/j.bbamem.2020.183467.

39. Mendelsohn, R., Mao, G., and Flach, C.R. (2010). Infrared reflection-absorption spectroscopy: principles and applications to lipid-protein interaction in Langmuir films. Biochim. Biophys. Acta *1798*, 788–800. https://doi.org/10.1016/j.bbamem.2009.11.024.

40. Vázquez, R.F., Daza Millone, M.A., Pavinatto, F.J., Fanani, M.L., Oliveira, O.N., Jr., Vela, M.E., and Maté, S.M. (2019). Impact of sphingomyelin acyl chain (16:0 vs 24:1) on the interfacial properties of Langmuir monolayers: A PM-IRRAS study. Colloids Surf. B Biointerfaces *173*, 549–556. https://doi.org/10.1016/j.colsurfb.2018.10.018.

41. Snyder, R.G., Aljibury, A.L., Strauss, H.L., Casal, H.L., Gough, K.M., and Murphy, W.F. (1984). Isolated C–H stretching vibrations of n-alkanes: Assignments and relation to structure. J. Chem. Phys. *81*, 5352–5361. https://doi.org/10.1063/1.447677.

42. Leverette, C.L., and Dluhy, R.A. (2004). Vibrational characterization of a planar-supported model bilayer system utilizing surface-enhanced Raman scattering (SERS) and infrared reflection–absorption spectroscopy (IRRAS). Colloids Surf. A: Physicochemical and Engineering Aspects *243*, 157–167. https://doi.org/10.1016/j.colsurfa.2004.05.020.

43. Arsov, Z., and Quaroni, L. (2008). Detection of lipid phase coexistence and lipid interactions in sphingomyelin/cholesterol membranes by ATR-FTIR spectroscopy. Biochim. Biophys. Acta *1778*, 880–889. https://doi.org/10.1016/j.bbamem.2007.12.012.

44. de la Arada, I., González-Ramírez, E.J., Alonso, A., Goñi, F.M., and Arrondo, J.L.R. (2020). Exploring polar headgroup interactions between sphingomyelin and ceramide with infrared spectroscopy. Sci. Rep. *10*, 17606. https://doi.org/10.1038/s41598-020-74781-8.

45. Hübner, W., and Blume, A. (1998). Interactions at the lipid–water interface. Chem. Phys. Lipids *96*, 99–123. https://doi.org/10.1016/S0009-3084(98)00083-8.

46. Villalaín, J., Ortiz, A., and Gómez-Fernández, J.C. (1988). Molecular interactions between sphingomyelin and phosphatidylcholine in phospholipid vesicles. Biochim. Biophys. Acta *941*, 55–62. https://doi.org/10.1016/0005-2736(88)90213-1.

47. Fookson, J.E., and Wallach, D.F. (1978). Structural differences among phosphatidylcholine, phosphatidylethanolamine, and mixed phosphatidylcholine/phosphatidylethanolamine multilayers: An infrared absorption study. Arch. Biochem. Biophys. *189*, 195–204. https://doi.org/10.1016/0003-9861(78)90132-7.

48. Goñi, F.M., and Arrondo, J.L. (1986). A study of phospholipid phosphate groups in model membranes by Fourier transform infrared

spectroscopy. Chem. Soc. *81*, 117–126. https://doi.org/10.1039/dc9868100117.

49. Levental, K.R., Surma, M.A., Skinkle, A.D., Lorent, J.H., Zhou, Y., Klose, C., Chang, J.T., Hancock, J.F., and Levental, I. (2017). w-3 polyunsaturated fatty acids direct differentiation ofthe membrane phenotype in mesenchymal stem cellsto potentiate osteogenesis. Sci. Adv. *3*, 1193. https://doi.org/10.1126/sciadv.aao1193.

50. Wassall, S.R., Leng, X., Canner, S.W., Pennington, E.R., Kinnun, J.J., Cavazos, A.T., Dadoo, S., Johnson, D., Heberle, F.A., Katsaras, J., and Shaikh, S.R. (2018). Docosahexaenoic acid regulates the formation of lipid rafts: A unified view from experiment and simulation. Biochim. Biophys. Acta. Biomembr. *1860*, 1985–1993. https://doi.org/10.1016/j.bbamem.2018.04.016.

51. Levental, K.R., Malmberg, E., Symons, J.L., Fan, Y.-Y., Chapkin, R.S., Ernst, R., and Levental, I. (2020). Lipidomic and biophysical homeostasis of mammalian membranes counteracts dietary lipid perturbations to maintain cellular fitness. Nat. Commun. *11*, 1339. https://doi.org/10.1038/s41467-020-15203-1.

52. Kim, W., McMurray, D.N., and Chapkin, R.S. (2010). n-3 polyunsaturated fatty acids– physiological relevance of dose. Prostaglandins Leukot. Essent. Fatty Acids *82*, 155–158. https://doi.org/10.1016/j.plefa.2010.02.028.

53. National Research Council (2011). Guide for the Care and Use of Laboratory Animals, Eighth Edition (Washington, DC: The National Academies Press).

54. Folch, J., Lees, M., and Sloane Stanley, G.H. (1957). A simple method for the isolation and purification of total lipides from animal tissues. J. Biol. Chem. *226*, 497–509. https://doi.org/10.1016/S0021-9258(18)64849-5.

55. Morrison, W.R., and Smith, L.M. (1964). Preparation of fatty acid methyl esters and dimethylacetals from lipids with boron fluoride–methanol. J. Lipid Res. *5*, 600–608. https://doi.org/10.1016/S0022-2275(20)40190-7.

56. Gaines, G.L. (1966). Insoluble Monolayers at Liquid–Gas Interfaces (Interscience Publishers, John Wiley & Sons).

57. Lheveder, C., Meunier, J., and Henon, S. (2000). Brewster angle microscopy. In Physical Chemistry of Biological Interfaces, A. Baszkin and W. Norde, eds. (Marcel Dekker, Inc.), pp. 560–574.

STAR★METHODS

KEY RESOURCES TABLE

REAGENT or RESOURCE	SOURCE	IDENTIFIER
Chemicals, peptides, and recombinant proteins		
1,2-dioleoyl-sn-glycero-3-phosphocholine (DOPC)	Avanti Polar Lipids	Cat#850375
N-palmitoyl-D-erythro-sphingosylphosphorylcholine (SM)	Avanti Polar Lipids	Cat#860584
Cholesterol (Chol)	Avanti Polar Lipids	Cat#700000
cis-4,7,10,13,16,19-Docosahexaenoic acid (DHA)	Sigma-Aldrich	Cat#D2534
1-stearoyl-2-docosahexaenoyl-sn-glycero-3-phosphocholine (SDPC)	Avanti Polar Lipids	Cat#850472
ω3 Regulip 1000	Raffo Laboratories, Argentina.	N/A
Experimental models: Organisms/strains		
Spontaneously Hypertensive Rats (SHR)	Charles River Breeding Laboratories	RRID:RGD_61000
Software and algorithms		
GraphPad Prism v9.1.2	Graph Path Software, Inc.	https://graphpad.com/
OriginLab Pro 2019b	OriginLab Corporation	https://originlab.com/

RESOURCE AVAILABILITY

Lead contact

Further information and requests for resources and reagents should be directed to and will be fulfilled by Sabina M. Maté (smate@med.unlp.edu.ar).

Materials availability

This study did not generate new unique reagents.

Data and code availability

- All data reported in the paper will be shared by the lead contact upon request.
- This paper does not report original code.
- Any additional information required to reanalyze the data reported in this paper is available from the lead contact upon reasonable request.

EXPERIMENTAL MODEL AND STUDY PARTICIPANT DETAILS

Spontaneously Hypertensive Rats (SHR, RRID: RGD_61000), bred in-house but originally derived from Charles River Breeding Laboratories (Wilmington, MA), were used in the study. Twenty-four male rats aged three weeks old were randomly divided into two groups, 12 members each, for control- and ω3-treatment. The animal housing room temperature was kept between 18°C and 24°C and humidity between 50 and 60%. The light was maintained on a 12-h, light-dark (7 am–7 pm) cycle. Rats were given daily handling, regularly weighing, and *ad libitum* access to water and food. All experimental procedures were reviewed and approved by the University of La Plata School of Medicine Animal Welfare Committee (CICUAL, protocol N° P04–01–2019) and performed following the Guide for the Care and Use of Laboratory Animals.

METHOD DETAILS

Materials

1,2-Dioleoyl-sn-glycero-3-phosphocholine (DOPC), N-palmitoyl-D-erythro-sphingosyl phosphorylcholine (16:0-SM), cholesterol (Chol) and 1-stearoyl-2-docosahexaenoyl-sn-glycero-3-phosphocholine (SDPC) were purchased from Avanti Polar Lipids (Birmingham, AL, USA), DHA was acquired from Sigma–Aldrich (St. Louis, MO, USA). All commercial lipids were used without further purification. Hepes buffer, NaCl, and other reagents, all analytical-grade, were acquired from Sigma–Aldrich (St. Louis, MO, USA). HPLC-grade chloroform was purchased from Merck (Darmstadt, Germany). All physical handling of lipids was performed in an inert atmosphere under low light conditions. All solvents and buffers that come into contact with SDPC and DHA were deoxygenated by bubbling with inert gas to carry away dissolved oxygen. SDPC and DHA were packaged into small aliquots, enabling the use of a fresh vial for every week of experimental work.

Animals and treatment

Three-week-old male SHR were housed in a temperature (18°C–24°C) and humidity (50–60%) controlled room, with a 12-h light/dark cycle (lights on: 07:00–19:00) and *ad libitum* access to water and food. SHR were randomly divided into two groups, as follows: untreated (SHR; n = 12), fed with standard laboratory rodent food and treated (SHR+ ω3; n = 12), supplemented orally with ω3 FAs (Regulip 1000, Argentinian product, Raffo Laboratories; each capsule of 1000 mg containing 180 mg eicosapentaenoic acid (EPA), 110 mg DHA and other ω3 FAs 45 mg) in dose 200 mg/kg body weight (BW)/day for 16 weeks. Control animals received water by the same via. This level of EPA/DHA is used pharmacologically for treating elevated triglycerides in human beings.[52] All experiments were performed following the Guide for the Care and Use of Laboratory Animals[53] and the experimental protocol (N° P04–01–2019) was approved by the Animal Welfare Committee (CICUAL), School of Medicine, UNLP.

Blood collection and cerebral cortex isolation

At the end of the treatment, the rats were anesthetized with sevoflurane and samples of cardiac blood were obtained. Then the animals were euthanized by rapid decapitation, and their brains were removed. Right hemispheres were dissected, and cortex was stored at $-$ 80°C for later lipids extraction.

Fatty acid analysis

Total plasma and cerebral cortex lipids were extracted according to the Folch method.[54] FA methyl esters from total lipids were obtained with BF_3-methanol according to the method of Morrison and Smith,[55] then analyzed by gas-liquid chromatography (GLC) in a Hewlett-Packard HP 6890 apparatus (Wilmington, DE) as described in.[37] Samples were injected into an Omegawax 250 (Supelco, Bellefonte, PA) capillary column of 30 m, 0.25 mm inner diameter, and 0.25 μm film thickness. The temperature was increased linearly at 3°C/min from 175°C to 230°C. The chromatographic peaks were identified by comparison of their retention times with those of authentic standards.

Surface pressure- area isotherms

Surface pressure measurements were carried out with a KSV Minitrough (KSV, Helsinki, Finland) using the Wilhelmy method. The aqueous subphase consisted of 20 mM Hepes, 150 mM NaCl, pH 7.4 (HBS Buffer) prepared in ultrapure water. The lipids (cerebral cortex- total lipid extracts or commercial lipids) dissolved in chloroform/methanol (2:1, v/v) were spread dropwise over the subphase surface with a Hamilton microsyringe. After 15 min of solvent evaporation and monolayer equilibration, the films were isometrically compressed at 5 cm²/min. The compressibility moduli (Cs^{-1}) of the films were calculated from the Surface pressure-Area isotherms according to Equation 1 [56]:

$$Cs^{-1} = - A(\partial \pi / \partial A)$$ (Equation 1)

where A is the mean molecular area at the surface pressure π.

All the surface pressure measurements were performed at 20 $\pm$ 1°C in triplicate.

Brewster Angle Microscopy (BAM)

Film imaging by BAM was performed with a Nanofilm EP3sw imaging ellipsometer (Accurion GmbH, Gottingen, Germany) operating at a resolution of 2 μm in the BAM mode. Minimum reflection was set with a polarized laser beam (λ = 532 nm) incident on the bare buffer surface (HBS buffer) at the experimentally calibrated Brewster angle (∼53.1°). The lipid monolayers were spread onto the aqueous surface and compressed as described before using a KSV Minitrough equipment (KSV, Helsinki, Finland). After monolayer formation and during compression, the reflected light was collected through a 20× objective to a CCD camera. The gray level at each pixel of the BAM images can be converted to reflectivity values with calibration factors tested for each individual experiment. The reflectivity obtained from BAM measurements is related to both the film thickness and refractive index of the film.[57] Therefore, the liquid expanded (Le) phases of lipid films appear as dark gray areas, whilst the more compact and thicker liquid ordered (Lo) phase is observed as light gray domains.

Polarization Modulation Infrared Reflection Absorption Spectroscopy (PM-IRRAS) experiments

PM-IRRAS measurements were performed using a KSV PMI 550 instrument (KSV, Biolin Scientific Oy, Espoo, Finland) coupled to a KSV Langmuir-Blodgett minitrough. The incoming light was continuously modulated at a high frequency between parallel (*s*-polarized) and perpendicular (*p*-polarized) with respect to the plane of incidence. Measurements were taken at an incident angle of 80°, at which positive bands indicate a transition moment oriented preferentially on the surface plane, whereas negative bands indicate preferential orientation perpendicular to the surface. An average of 6000 scans was collected for each spectrum at a resolution of 8 cm^{-1} using the corresponding subphase (HBS buffer) spectrum as background. The films were formed by spreading the synthetic lipid mixtures dissolved in chloroform on the subphase surface. After solvent evaporation and monolayer equilibration (15 min), the monolayers were compressed at 5 cm²/min to a surface pressure of 30 mN/m and PM-IRRAS spectra were collected. Measurements were conducted in a class 10,000 clean room at 20 $\pm$ 1°C and were performed in triplicate.

AFM imaging and force spectroscopy measurements

Sample preparation

The cerebral cortex-total lipid extracts were dissolved in a mixture of chloroform:methanol (2:1, v/v) to a concentration of 10 mg/mL. Dried lipid films were then prepared on the walls of a tube by evaporation of the solvent under a gentle stream of dry nitrogen and left overnight under vacuum, covered from light. The films were hydrated with "working buffer" (25 mM Hepes buffer, pH 7.6, 150 mM NaCl) at 70°C to a final concentration of 0.5 mg/mL and subjected to 5 cycles of vortex mixing and heating. The vesicle suspensions were placed in an ultrasound bath for 30 min and extruded through a 100 nm pore-size polycarbonate membrane to finally obtain unilamellar vesicles. Supported lipid bilayers (SLBs) were obtained by direct vesicle fusion onto freshly cleaved mica surfaces (mica discs, Ted Pella, Redding, CA). Ten µL of buffer including Ca^{2+} ions (25 mM Hepes buffer, pH 7.6, 150 mM NaCl, 3 mM $CaCl_2$) were placed onto the mica surface, followed by the incubation of 100 µL of vesicles suspension (0.5 mg/mL) for 30 min at 60°C. The samples were left to cool to room temperature and rinsed several times with working buffer to remove unfused vesicles, keeping always the samples hydrated.

AFM imaging and force spectroscopy

The experiments were performed with a NanoWizard 3 BioScience atomic force microscope (AFM) (JPK Instruments, Bruker Nano GmbH) at room temperature and under liquid environment (working buffer). Silicon nitride probes with nominal spring constant of 0.1 N/m (MLCT-BIO DC-E, Bruker) were used. After having measured the sensitivity (V/m), the cantilever spring constants were individually calibrated using the equipartition theorem (thermal noise routine). Imaging was performed in the Quantitative Imaging (QI^{TM}) mode, with 200 pN setpoint, a total Z length of 50 nm, and 30 µm/s velocity. Force-distance curves (contact mode) were recorded by approaching and retracting the AFM tip at constant velocity (1 µm/s) to a setpoint of 9 nN, and in the force map mode of 16 x 16 force-separation curves over previously visualized areas. AFM data were acquired and processed using the JPK AFM software. The breakthrough force, F_b, was recorded from each approach trace, computing the difference in force between the point of contact and the onset of sudden penetration. Statistical analysis and representation of the data was performed with GraphPad Prism 9.1.2 or OriginPro2019b. Errors are indicated as standard deviation.

QUANTIFICATION AND STATISTICAL ANALYSIS

Statistical details are provided in the figure captions and method details section. The value of n represents the number of replicates in each experiment. Unless otherwise stated, results are reported as mean ± SD. Tests were accomplished at the 0.05 level (cut-off for significance).